Peridynamic simulations of damage in indentation and scratching of 3C-SiC

Yimeng Xu
Beijing Institute of Technology
Pengzhe Zhu (pzzhu@bit.edu.cn)
Beijing Institute of Technology https://orcid.org/0000-0001-9844-4280

Research Article

Keywords: Peridynamics, 3C-SiC, Indentation, Scratch, Damage

Posted Date: May 12th, 2022

DOI: https://doi.org/10.21203/rs.3.rs-1552808/v1

Peridynamic simulations of damage in indentation and scratching of 3C-SiC

Yimeng Xu, Pengzhe Zhu*

School of Mechanical Engineering, Beijing Institute of Technology, Beijing 100081, China

*Corresponding author: Pengzhe Zhu, Email: pzzhu@bit.edu.cn

Abstract

The cubic silicon carbide (3C-SiC) has broad application prospects in many fields due to its excellent material properties. The modeling of damage in 3C-SiC due to contact loads is important yet challenging. In this paper, simulations based on ordinary state-based peridynamics (PD) theory are proposed to model the damage of 3C-SiC in indentation and scratching. The constitutive parameters of 3C-SiC for PD simulation are obtained by performing MD simulations of nanoindentation. It is found that in the indentation simulations the initiation and propagation of cracks are observed, which shows that the PD can model the crack formation and propagation in the indentation process of brittle solid materials. During the scratching process, the variation of friction force is consistent with that of material wear. It is also found that the specific cutting energy increases nonlinearly with the decrease of scratching depth due to size effect. In addition, for the scratching with double indenters, the volume of material removal is more than twice that of scratching with an indenter due to the coupling effect of the two indenters under certain conditions. This paper demonstrates that PD is a powerful tool to investigate the indentation and scratching process of brittle solid materials.

Keyword: Peridynamics; 3C-SiC; Indentation; Scratch; Damage

1. Introduction

The cubic silicon carbide (3C-SiC) has broad application prospects in many fields such as microelectromechanical systems (MEMS), laser, detection and other optoelectronic devices due to its excellent mechanical, chemical, electrical and thermal properties [1-3]. In most applications, SiC materials have to undergo contact loads inevitably, which will lead to damage such as cracks in SiC that deteriorate the mechanical properties of SiC devices [4]. So, it is fundamentally important to understand the damage characteristics in the indentation and scratching process of 3C-SiC.

At present, a great number of experiments [5-8] and simulations [9-13] have been carried out to investigate the deformation mechanisms of 3C-SiC. For instance,

Mishra *et al.* performed large-scale molecular dynamics (MD) simulations of nanoindentation and found that the primary deformation mechanisms of 3C-SiC are dislocation nucleation and propagation in the low pressure (zincblende) phase [11]. Goel *et al.* investigated the influence of crystal anisotropy of 3C–SiC during its cutting behavior by MD simulations [12]. Liao *et al.* employed MD simulations to analyze the elastic-plastic deformation law of 3C-SiC ceramic parts with hemispherical and regular pyramid indenters under ultimate loads and analyzed the evolution of dislocations in nanoindentation [13]. Although great insights into the deformation and damage of 3C-SiC have been gained using MD simulations, MD simulations usually fail to capture the spatial and temporal scales in experiments due to the high computational cost. Therefore, many simulation methods based on classical continuum mechanics (CCM) such as finite element method (FEM) [14] and smooth particle hydrodynamics (SPH) have been adopted to study the indentation and scratching of SiC [15]. For example, Shim *et al.* investigated the plastic flow behavior of SiC under nanoindentation by FEM [16]. Zhang *et al.* performed FEM simulations together with corresponding experimental validations to reveal the synergetic deformation behavior between SiC matrix and Si particle under vibration-assisted diamond cutting [17]. Zhao *et al.* employed FEM and experiments to reveal the coexistence of microscopic plastic deformation and brittle fracture of 3C-SiC at different indentation depths [18]. The scratching process of SiC was also investigated using SPH [19,20]. However, the FEM and SPH are based on continuum approaches and cannot properly deal with the discontinuity problems such as crack initiation and propagation occurring in the indentation and scratching of SiC [21].

Given the limitations of existing methods for simulating discontinuity problems such as crack initiation and propagation, peridynamics (PD) as a new nonlocal theory developed by Silling *et al.* [22] provides a more refined approach for materials damage analysis. The PD employs the integral equations of motion instead of the conventional spatial differential equations, thus overcoming the challenges of modeling the discontinuity problems with spatial differential equations used in CCM.In fact, PD theory has been widely used in various fields to deal with discontinuity problems, including quasi-static fracture problems [23], dynamic fracture of brittle materials [24,25], composites cutting [26,27] and impact [28,29], fatigue cracking [30], heat conduction phenomena [31,32] *etc.* Cao *et al.* used PD simulations to describe the nanoindentation of an archetypical soda-lime silicate window glass [33]. Sayna *et al.* [34] adopted two-dimensional state-based PD model to study the nanoscale friction and wear behaviors of thin amorphous carbon films. However, little attention has been paid to the scratching process, especially for SiC materials. The ability of PD to properly describe the response to indentation and scratching of 3C-SiC is yet to be explored. To address this issue, in this paper, 3C-SiC indentation and scratching simulations are carried out using PD method. The results of PD are in good agreement with those of MD as well as experiments. This study demonstrates that PD method is a powerful tool to investigate the damage evolution in indentation and scratching of 3C-SiC. It can also provide a reference for the modeling of damage evolution of other brittle materials.

2. PD Methods

PD theory employs a finite number of particles to discretize a solid. The equations of motion in PD theory are given by Eq. (1) [35].

$$\rho \ddot{\mathbf{u}}(\mathbf{x},t) = \int_{H_x} \left\{ \underline{\mathbf{T}}[\mathbf{x},t]\left\langle \mathbf{x}' - \mathbf{x} \right\rangle - \underline{\mathbf{T}}\left[\mathbf{x}',t\right]\left\langle \mathbf{x} - \mathbf{x}' \right\rangle \right\} dV_{x'} + \mathbf{b}(\mathbf{x},t) \tag{1}$$

where ρ is the material mass density, H_x is the domain of the spherical horizon with a radius δ, $\underline{\mathbf{T}}$ is the force vector state field, $\mathbf{b}$ is the body force density field, t is the time and $dV_{x'}$ is the volume of a particle.

A short-range force model has been introduced to describe the interaction between indenter and substrate [36]. The contact force is independent of the initial distance between material particles, only depending on the current relative positions of particles. The short-range force density between material particles p and i is defined by Eq. (2).

$$f_s\left(\mathbf{y}_p, \mathbf{y}_i\right) = \begin{cases} \dfrac{c_{sh}}{\delta}\left(\left\|\mathbf{y}_p - \mathbf{y}_i\right\| - d_{pi}\right)\dfrac{\mathbf{y}_p - \mathbf{y}_i}{\left\|\mathbf{y}_p - \mathbf{y}_i\right\|}, & \text{if } \left\|\mathbf{y}_p - \mathbf{y}_i\right\|,, d_{pi} \\ 0, \quad if \left\|\mathbf{y}_p - \mathbf{y}_i\right\| > d_{pi} \end{cases} \tag{2}$$

where $c_{sh} =$ 15c, and $c = 12E / (\pi\delta^4)$is a peridynamic modulus. d_{pi} is the critical distance to determine the contact.

$$d_{pi} = \min\left\{0.9\left\|\mathbf{x}_p - \mathbf{x}_i\right\|, 1.35\left(r_p + r_i\right)\right\} \tag{3}$$

where $\boldsymbol{x}_p$ and r_p are the position and radius of particle p in the vicinity of particle i, respectively. r_i is the radius of particle i, which is set equal to one-half of the grid size.

Considering the Coulomb law, the constitutive model for friction is defined by Eq. (4) [37,38].

$$R_{\mathrm{fric}}(v, f) = c_{\mathrm{fric}} f \min\left\{\frac{v}{\dot{o}_{\mathrm{fric}}}, 1\right\} \tag{4}$$

where $\mathrm{c}_{\mathrm{fric}}$ is a regularization parameter with dimensions of speed (indicating the maximum slip speed that is allowed in the static friction regime), and c_{fric} is the coefficient of friction. During the simulation, the friction force can be obtained by considering the contact force and friction coefficient.

Local damage at a point is defined as the weighted ratio of the number of eliminated interactions to the total number of initial interactions of a material particle with its family members. To describe the degree of the local damage of material particles, by using statistical methods, the damage D is defined by Eq. (5) [36,39].

$$D(\mathbf{x},t) = 1 - \frac{\int_H \mu\left(\mathbf{x}' - \mathbf{x}, t\right) dV'}{\int_H dV'} \tag{5}$$

where μ is a scalar-valued function and also a discontinuous function to characterize whether the bond between two material particles is broken. When the fracture occurs, μ is 0; otherwise, μ equals 1. The local damage at a point can be quantified as a value which ranges from zero to one [36]. When the local damage is one, all the interactions initially associated with the point have been eliminated. While a local damage of zero means that all interactions are intact. The measure of local damage is an indicator of possible crack formation within a body.

In this paper, the open-source software Peridigm is employed for PD simulations [40].

2.1 Indentation

The indentation model consists of a diamond indenter and a 3C-SiC substrate. An ordinary state-based PD model of 3C-SiC substrate with dimensions of 297×297×297 μm^3 is considered, as shown in Fig.1(a). The interparticle distance is 3.3 μm. This study intends to observe the damage evolution in the indentation process. Therefore, the elastoplastic constitutive model of 3C-SiC was parameterized based on existing experimental data. Specifically, the density of 3C-SiC substrate is set to 3200kg/m^3 and Poisson's ratio is set to 0.168 [41]. Young's modulus and yield stress used herein are obtained by performing MD simulations, as shown in Figure S-2. Thus, this can ensure a meaningful comparison between multiscale simulations and experiments. Here, Young's modulus and yield stress of SiC substrate are 320 GPa and 64.7 GPa, respectively. Then a hemispherical diamond indenter model with a radius of 30 μm is established. The elastic constitutive model is adopted for the indenter and the materials parameters are: Young's modulus E = 1143 GPa, Poisson's ratio v = 0.0691 and density ρ = 3515 kg/m^3 [42].

Similar to the previous studies [43], the horizon δ is 3.05 times the interparticle distance and the critical stretch is set to be 5×10^{-4}. The particles in the bottom are fixed to serve as the boundary to anchor the 3C-SiC substrate. The timestep is set as 50 ps, which is small enough to ensure the stability of the simulations based on stability analysis [36].

At the beginning of the indentation simulation, the indenter is above the substrate. Then the indenter indents with a fixed speed (loading) until the maximum indentation depth (15 μm) is reached. Subsequently, the indenter moves upward with the same fixed speed (unloading). The load is computed as the resultant force applied by the indenter on the substrate. Specifically, all the individual components of force applied on the indenter at a given moment are recorded and then added up to calculate the resultant force. Different indentation speeds of 1 m/s, 5 m/s, 10 m/s and 20 m/s are also employed to further study the effect of indentation speed on the deformation mechanism of materials.

2.2 Scratching

The material and key parameters of the PD scratching model are the same as those of the indentation model. The 3C-SiC scratching model with a size of 594×198×198 μm^3 is established. The indenter parameters remain the same as those in the indentation,

as shown in Fig.1(b). The indenter indents to a certain depth of the substrate, and then scratches the substrate along the negative x direction with a fixed speed. The coefficient of friction between the substrate and the indenter is set as 0.15 [44]. The total scratching distance is 350 μm.

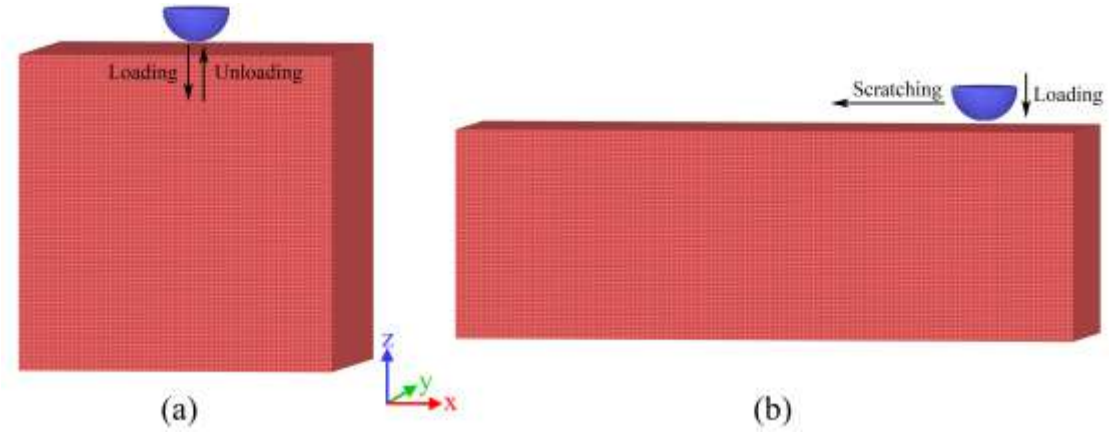

Fig.1. PD model (a)indentation model, (b)scratching model.

To quantitatively analyze the scratching process, the friction force, wear volume and specific cutting energy during scratching are calculated. The friction force is obtained by summing up the individual forces on the indenter particles along the x direction during the simulation. The wear volume is defined as $\sum D \cdot V$, where D and V are the damage and volume of the particles, respectively. The power during scratching is calculated by $W = F \cdot v$, and the trapezoidal integral method is used to integrate the time to obtain the cutting energy. Combined with the wear volume obtained previously, the specific cutting energy can be obtained by Eq. (6).

$$SCE = \frac{\int Fvdt}{\sum DV} \tag{6}$$

To explore the influence of scratching depth, the scratching depths of 1 μm, 2 μm and 3 μm are selected for the simulations. To investigate the effect of scratching speed, different scratching speeds of 1 m/s, 10 m/s, 20 m/s and 40 m/s are chosen for two typical scratching depths of 1 μm and 3 μm.

In the actual grinding process, multiple abrasives are present on the grinding wheel. Different abrasives produce different scratches, which may interact with each other. Therefore, to investigate the interaction of the different abrasives, scratching simulations with double indenters at different intervals are also conducted. The indenter intervals are 40 μm, 50 μm and 60 μm, respectively, for the double-indenter mode. In this case, a typical scratching depth of 3 μm is chosen to better compare the results of a single indenter with those of double indenters. The details of the PD model and simulation parameters are shown in Table 1.

Table 1 Details of the PD model and simulation parameters.

Configuration	PD simulation
Substrate materials	3C-SiC
Substrate constitutive model	State-Based Elastic Plastic
Substrate Young's modulus	From MD

Substrate Poisson's ratio v	0.168
Substrate Density	3200 kg/m³
Substrate Yield stress	From MD
Indenter materials	Diamond
Indenter constitutive model	State-Based Elastic
Indenter radius	30 μm
Indenter Young's modulus	1143 GPa
Indenter Poisson's ratio v	0.0691
Indenter Density	3515 kg/m³
Coefficient of friction	0.15
Indenter radius	30 μm
Critical stretch	5×10^{-4}
Interparticle distance	3.3 μm
Horizon δ	10.065 μm
Time step	50 ps

3. Results and discussions

3.1 Indentation simulations

The load–depth curves of the PD indentation simulation at different indentation speeds are shown in Fig.2 In the process of loading, the "pop-in" phenomenon can be observed. For the indentation speeds of 5 m/s, 10 m/s and 20 m/s, the load-depth curves in the loading process almost completely overlap. However, the load exhibits a certain degree of decrease when the indentation speed decreases to 1 m/s. In the unloading process, the load decreases faster for a higher indentation speed.

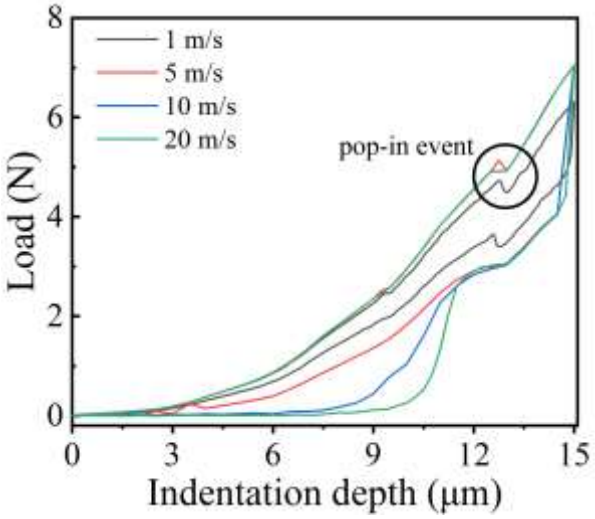

Fig.2. The load–depth curves of the indentation using PD simulation.

The damage of substrate during indentation is almost the same for speeds of 5 m/s, 10 m/s and 20 m/s. Therefore, the simulation results with a speed of 5 m/s are taken as the representative at these three speeds and compared with those at 1 m/s. The top view and sectional view of the 3C-SiC are shown in Fig.3 and Fig.4, respectively. It can be found that with the increase of indentation depth, the

displacement field and damage area gradually expand in all directions. When the indentation speed is 1 m/s, the damage is small and the damage area has good central symmetry. When the indentation speed reaches 5 m/s, the displacement of the substrate is larger and the symmetry of crack propagation begins to be destroyed. Four cracks with different lengths can be observed in Fig.4. The cracks in the inner part of the substrate propagate asymmetrically to the surrounding. The obvious propagation of cracks appears in the 45° direction. The initiation and propagation of cracks in the PD simulation are in good agreement with those of existing SiC indentation tests [45], which indicates the effectiveness of the PD indentation model of 3C-SiC.

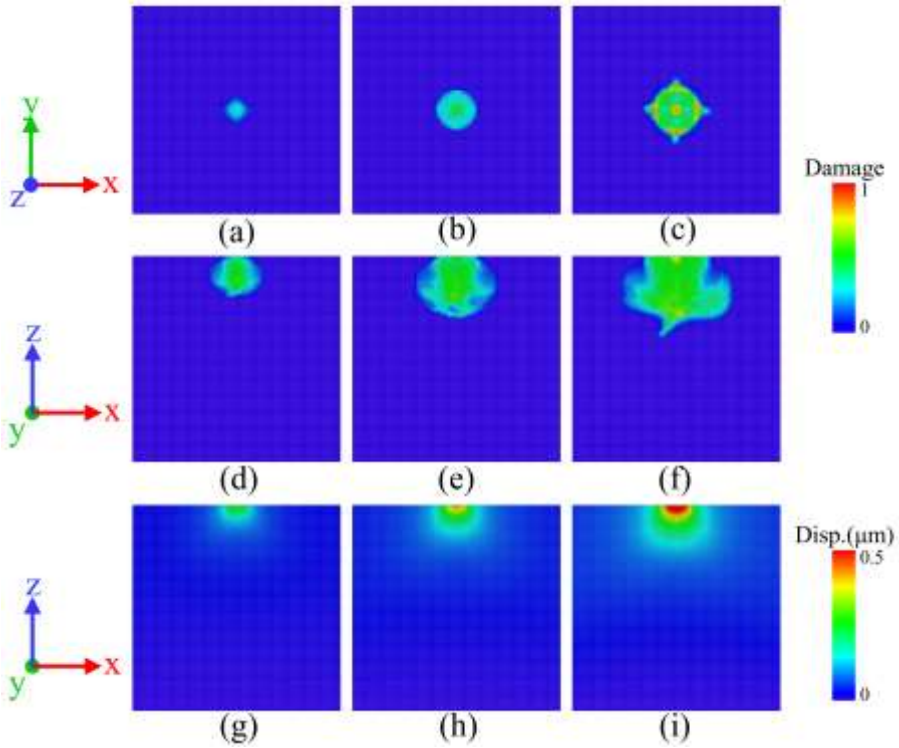

Fig.3. Damage and displacement contours of 3C-SiC substrate at 1 m/s. Top view of the substrate at the indentation depths of (a) 10 μm, (b) 13 μm and (c) 15 μm. Sectional view of the substrate at the indentation depths of (d,g) 10 μm, (e,h) 13 μm and (f,i) 15 μm.

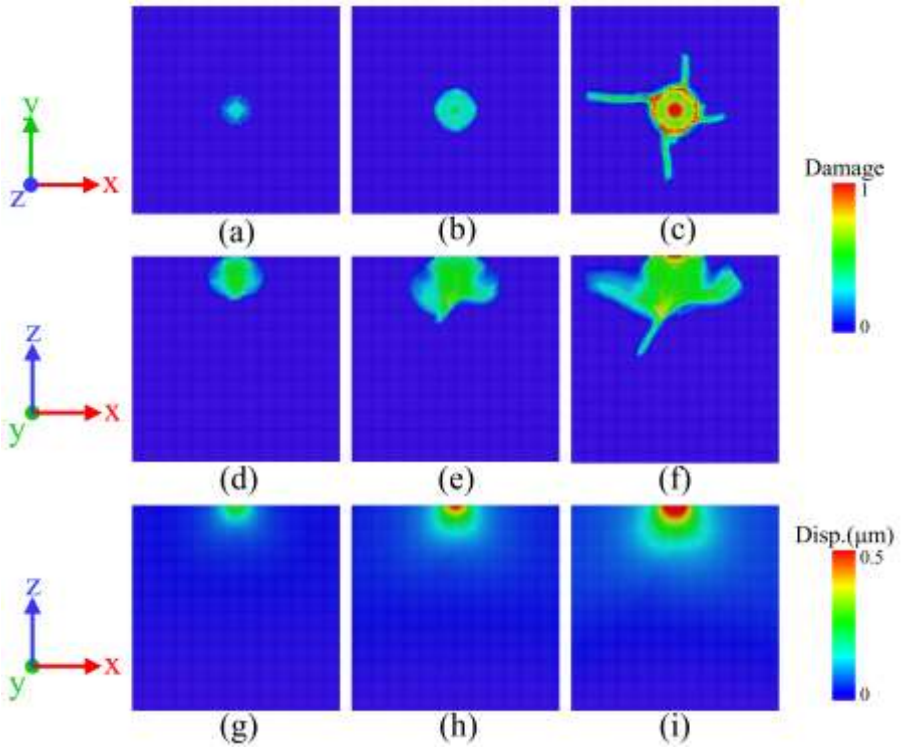

Fig.4. Damage and displacement contours of 3C-SiC substrate at 5 m/s. Top view of the substrate at the indentation depths of (a) 10 μm, (b) 13 μm and (c) 15 μm. Sectional view of the substrate at the indentation depths of (d,g) 10 μm, (e,h) 13 μm and (f,i) 15 μm.

3.2 Scratching simulations

3.2.1 Scratching with a single indenter

The scratching process is first simulated with a single indenter. The friction force and normal force in the scratching process at different scratching depths are shown in Fig.5. It can be found that the variations of friction force and normal force have a similar trend. The maximum friction force and normal force increase with the increase of scratching depth. At the scratching depths of 1 μm and 2 μm, the friction force and normal force show very slight variations in the scratching process. However, at the scratching depth of 3 μm, the friction force and normal force showed cyclic fluctuations with seven distinct cycles occurring during the scratching process. The big fluctuations of friction and normal force during scratching are similar to the variations of the cutting forces in the cutting simulations using PD [21]. In addition, the wear volume during the scratching process at different depths is also calculated, as shown in Fig.6(a). The wear volume increases nonlinearly with the scratching depth. When the scratching depth is 1 μm and 2 μm, the wear volume increases smoothly with the scratching distance. However, as the scratching depth increases to 3 μm, the variation of the wear volume exhibits seven cycles.

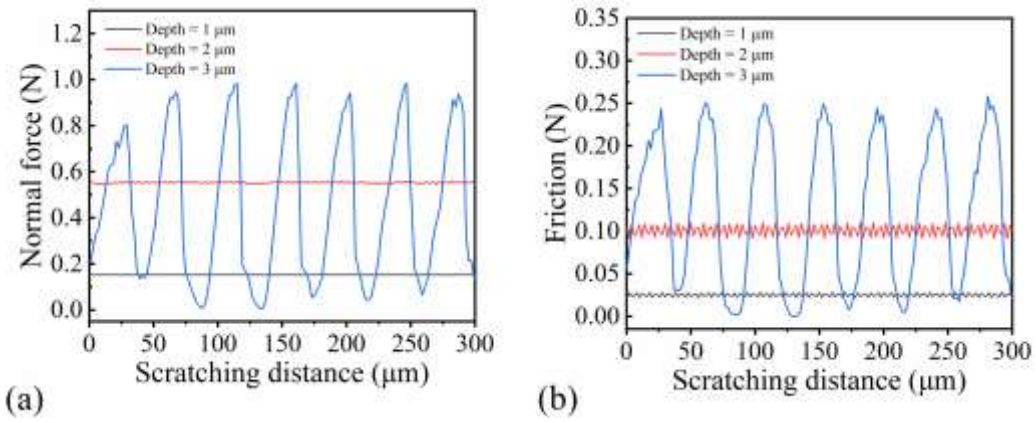

Fig.5. (a) Normal force and (b) friction of PD scratching simulation at different depths

By calculating the total damage value added by each step, it can be found that the occurrence of wear is consistent with the variation of the force curve, as shown in Fig.6(b). This demonstrated that the variation of the friction force is highly correlated with damage formation.

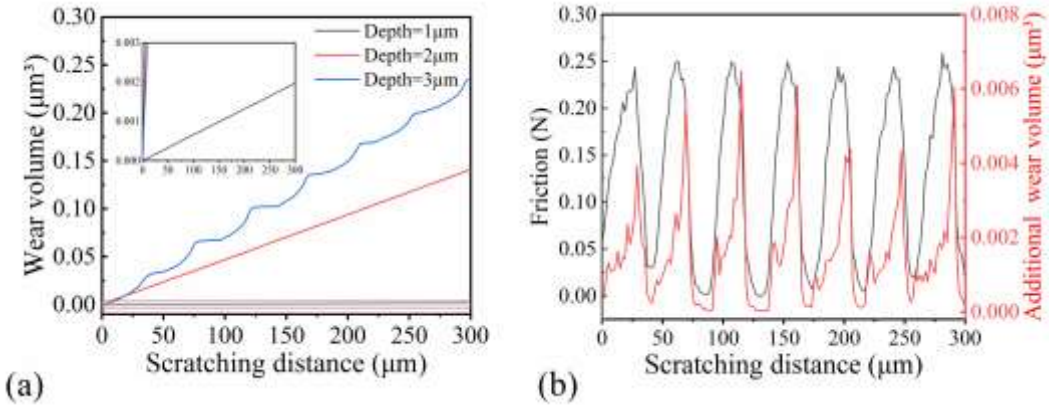

Fig.6. (a) Wear volume at different depths; (b)Variations of friction and the occurrence of wear.

The damage contours of the substrate at different scratching depths are also shown in Fig.7. With the increase of scratching depth, the number of severely damaged particles gradually becomes greater and the damage range expands. It can be seen that at a scratching depth of 1 μm, the width and depth of the scratch are small and insignificant, see Fig.7(a). When the scratching depth increases to 2 μm, a smooth scratched surface appears, and both the depth and width experience a significant increase, see Fig.7(b). When the scratching depth further increases to 3 μm, the width and depth of the scratch increase and the damage with seven periodic shapes appears during the 300 μm scratching distance, as shown in Fig.7(c).

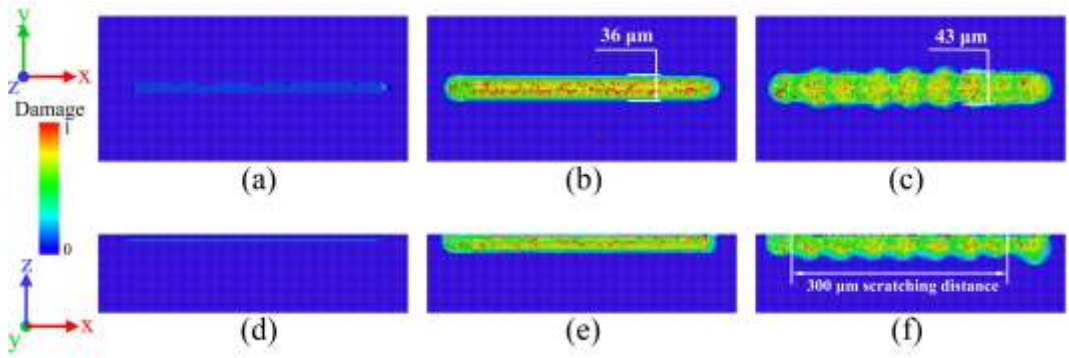

Fig.7. Damage contours of substrate at scratching depths of (a,d) 1 μm, (b,e) 2 μm and (c,f) 3 μm.

The displacement field and damage contours of the substrate during the scratching process are also shown in Fig.8. As the indenter moves forward, the part of the substrate surface in contact with the indenter is deformed. Some particles are scratched by the indenter and grooves are formed in the substrate. When the scratching depth is small (less than 2 μm), the displacements of substrate particles occur mainly in the lower front of the indenter and remain stable throughout the scratching process. This allows the scratch to remain smooth. When the scratching depth increases to 3 μm, the displacements of substrate particles around the indenter start to show periodic variations. As shown in Fig.8(e,f), when the scratching distance is 130 μm, the displacements of the substrate under the indenter are even smaller than those of the substrate at a scratching depth of 2 μm. As the indenter continues to move forward, the displacement of substrate particles becomes gradually greater and reaches the biggest at a scratching distance of 150 μm. At this time, the damage occurs in a larger area in front of the indenter, and the friction is near the peak. Then the displacements of substrate particles gradually become smaller and move to the next cycle. For the scratching depth of 3 μm, the periodic change of displacement field is the reason for the cyclic change of force as well as damage.

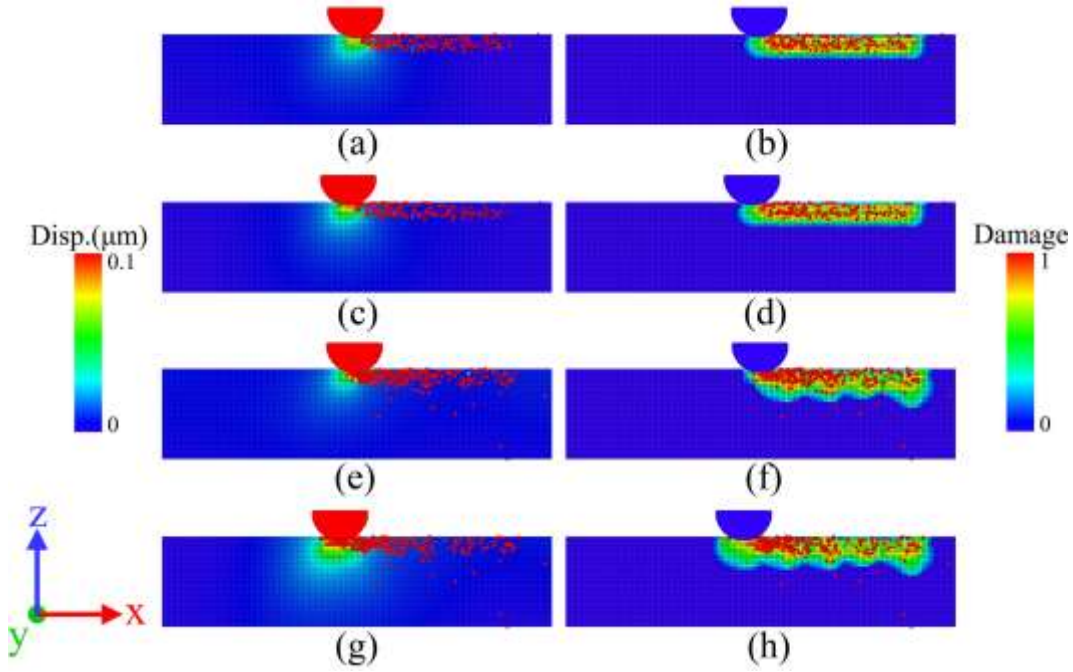

Fig.8. Displacement field and damage contours during scratching process with (a,b) depth = 2 μm, distance = 130 μm; (c,d) depth= 2 μm, distance = 150 μm; (e,f) depth = 3 μm, distance = 130 μm; (g,h) depth = 3 μm, distance = 150 μm.

To further study the effect of scratching depth, the specific cutting energy is obtained, as shown in Fig.9. It can be seen that the specific cutting energy increases nonlinearly as the scratching depths decrease. When the scratching depth is 1 μm, the specific cutting energy fluctuates around 22 GPa, which is much larger than that for a larger scratching depth. In the 3C-SiC scratching experiment, size effect is a main reason for the nonlinear increase of specific cutting energy with the decrease of scratching depth, which is consistent with simulation results [6].

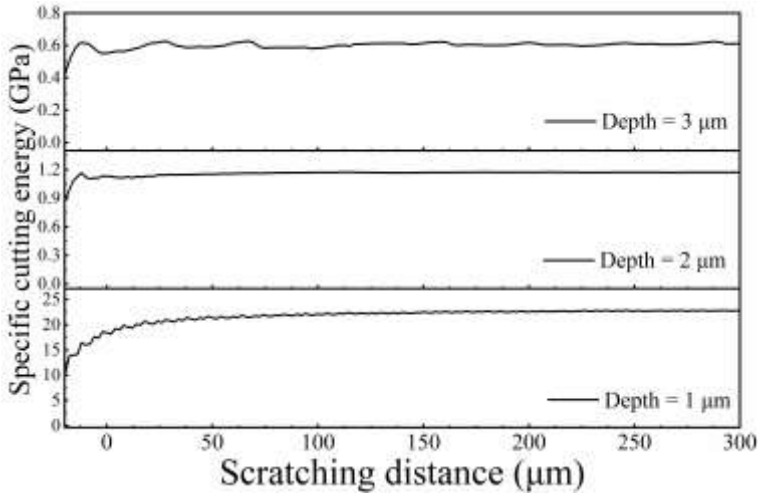

Fig.9. Specific cutting energy at different scratching depths.

3.2.2 Scratching with double indenters

The force curves of the PD scratching simulations for double indenters with different intervals of 40 μm, 50 μm and 60 μm are shown in Fig.S-7. The friction and normal force for scratching with double indenters showed no significant difference in the magnitude of the average values throughout the scratching process at different intervals.

Fig.10 shows the damage contours for different indenter intervals. It can be found from Fig.10(c) that when the interval is 60 μm, two scratches are presented and the width of each scratch is equal to that of the single indenter with the same parameters. For the interval of 50 μm, the scratch also shows a clear periodicity and the scratch width is about 92 μm, which is more than twice the width of the single indenter, as shown in Fig.10(b). When the indenter interval continues to decrease to 40 μm, the scratch width decreases, and the scratch exhibits irregular undulation instead of periodicity, see Fig.10(a). In other words, for the same scratch depth, the region of interaction between adjacent scratches depends on the indenter interval. The area of interaction between adjacent scratches increases first and then decreases as indenter interval increases.

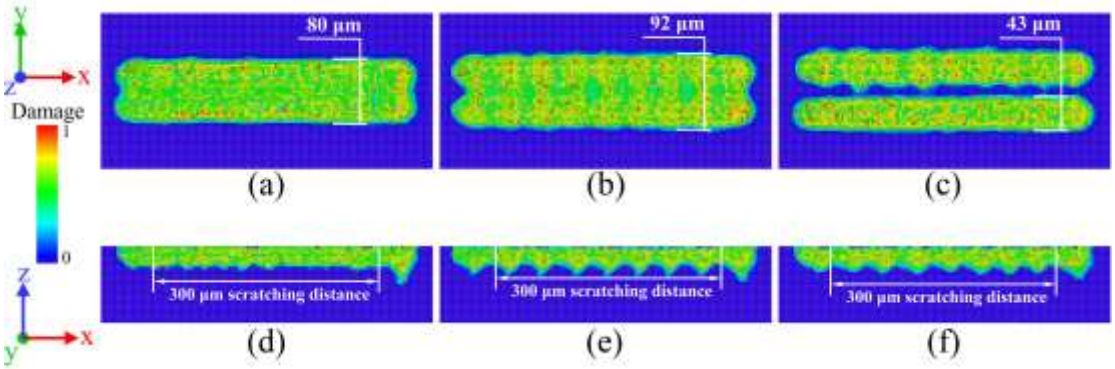

Fig.10. Damage contours of the substrate during scratching for double indenters with indenter intervals of (a,d) 40 μm, (b,e) 50 μm and (c,f) 60 μm.

The total wear volume at different indenter intervals is also counted, as shown in Fig.11(a). It can be seen that when the interval is 60 μm, the total wear volume is almost twice the wear volume of the single indenter. When the interval is 50 μm, there is a significant increase in wear volume compared to the 60 μm interval. When the interval is 40 μm, the wear volume is slightly larger than that of the 60 μm interval and less than that of the 50 μm interval. We further calculate the specific cutting energy at different intervals, as shown in Fig.11(b). It can be found that the maximum cutting specific energy at the interval of 60 μm is around 0.6 GPa, which is consistent with that for the single indenter with the same parameters. The scratching for 50 μm interval has the smallest cutting specific energy, which facilitates the material removal and leads to the maximum wear volume. The scratching for 40 μm interval has a slightly lower cutting specific energy compared to that of 60μm interval, which also results in a slightly larger wear volume.

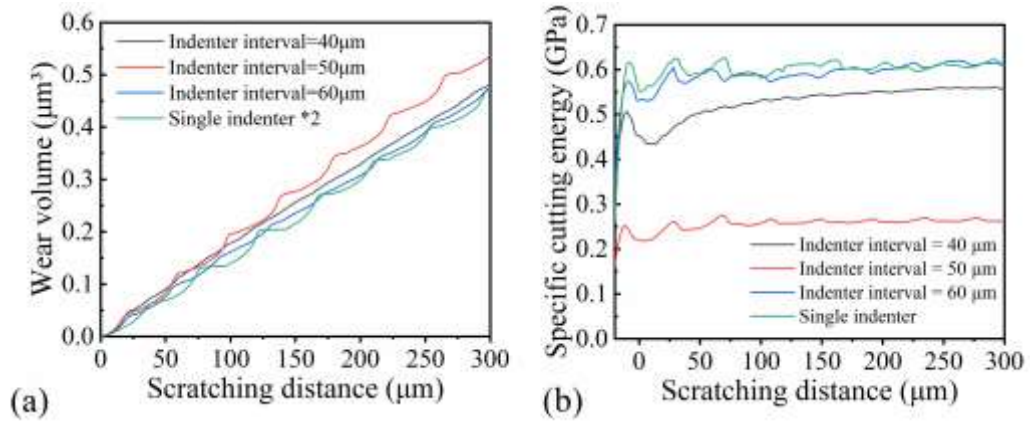

Fig.11. (a)wear volume and (b)specific cutting energy during scratching under the double indenters at different indenter intervals.

Fig.12. shows the sectional view of the substrate in scratching. It can be found that when the indenter interval is 60 μm, two separate scratches appear, see Fig.12(c). As shown in Fig.12(b), when the indenter interval is reduced to 50 μm, the superposition of the displacement field makes the scratches overlap and the damage area increases significantly. As the indenter interval continues to decrease to 40 μm, the scratches still overlap, but the damage area is reduced compared to the case with indenter interval of 50 μm, see Fig.12(a).

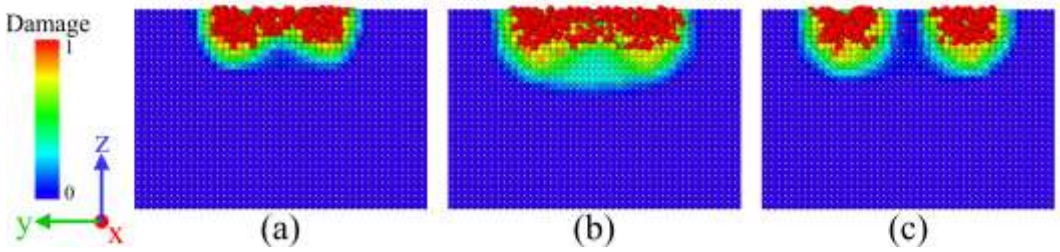

Fig.12. Side sectional view damage contours under double indenter scratching with indenter intervals of (a) 40 μm, (b) 50 μm and (c) 60 μm.

In general, the interaction between adjacent scratches depends on the indenter interval. When the scratching depth is 3 μm and the indenter interval is less than 50 μm, there is an interaction between the two indenters due to the superposition of the displacement field generated in the scratching. The volume of material removed by two scratches is more than twice that of a single scratch. This is attributed to the superposition of the displacement field that can lead to interaction-induced material removal caused by cracks between two scratches and the reduction of specific cutting energy. Moreover, there is a critical interval at which the volume of material removed reaches its peak. This is because the total influence region of the displacement field decreases as the two indenters get too close. Meanwhile, the interaction of damage between adjacent scratches becomes weaker as the indenter interval is large enough due to the limited diffusion length of the damage [46]. Therefore, when the indenter interval is large enough, the interaction between pairs of scratches does not exist. The results are consistent with the existing experimental results [46].

According to the study above, 3C-SiC has different removal phenomena at different scratching depths. Therefore, to study the effect of scratching speed, the scratching depth of 1 μm and 3 μm are chosen. In this work different scratching speeds of 1 m/s, 10 m/s, 20 m/s, and 40 m/s are adopted. The simulation results are shown in Fig.S-3~S-6. It is reasonable that, at the scratching depth of 1 μm, the scratching speed has almost no effect on the scratching phenomenon. However, in the case of scratching depth of 3 μm, the friction and normal forces remain almost the same in the range of speeds studied. When the scratching speed is reduced to a certain level (1 m/s), the amplitude of the friction and normal forces decreases, but the average value is almost the same. At the same time, the amount of wear and specific cutting energy maintain the same levels in the range of scratching speeds studied.

4. Conclusions

In this paper, an ordinary state-based PD theory is employed to model the indentation and scratching process of 3C-SiC. The constitutive parameters of 3C-SiC for PD simulation are obtained by performing MD simulations of nanoindentation. The PD simulation results are in good agreement with experimental results. The main conclusions are drawn as follows:

(1) In the PD simulations of the indentation process, the initiation and propagation of cracks in 3C-SiC are reproduced, which clearly shows that the PD can successfully model the crack formation and propagation in the indentation process of

brittle solid materials.

(2) During the scratching process, the variation of friction is consistent with that of material wear. The wear volume increases significantly with the increase of the scratching depth. However, the specific cutting energy increases nonlinearly with the decrease of the scratching depth due to size effect.

(3) For the scratching with double indenters, the material removal is greatly affected by the indenter interval. The volume of material removal by two indenters in the scratching is more than twice that of one indenter due to the coupling effect of the two indenters when the indenter interval is less than the critical distance.

In this paper, the implementation of PD theory for the indentation and scratching simulations of a typical brittle solid material (3C-SiC) has been carried out. This study provides detailed parameters for PD indentation and scratching models. The methods for constructing PD indentation and scratching models developed in this paper can be extended to other brittle materials. This paper shows that the dynamic damage evolution in the indentation and scratching of brittle materials can be captured by PD method. Overall, this work demonstrates that PD is a powerful tool to investigate the indentation and scratching process of brittle solid materials

Statements and Declarations

·Funding: This work is supported by **Beijing Natural Science Foundation (Nos. L212025 and 3202024), NSAF (No.U2130108), National Natural Science Foundation of China (No. 51875405), Tribology Science Fund of State Key Laboratory of Tribology(No. SKLTKF20B13) and Beijing Institute of Technology Research Fund Program for Young Scholars.**

·Conflict of Interests: The authors declare that they have no conflict of interest.

·Data availability: The raw/processed data required to reproduce these findings cannot be shared at this time as the data also forms part of an ongoing study.

References

[1] Talwar, D. N., and Joseph C. Sherbondy. Thermal expansion coefficient of 3C–SiC. Applied Physics Letters 67,22 (1995): 3301-3303.

[2] Guo, Han, et al. Epitaxial growth and electrical performance of graphene/3C–SiC films by laser CVD. Journal of Alloys and Compounds 826, (2020): 154198.

[3] Biscay, Nicolas, et al. Behavior of silicon carbide materials under dry to hydrothermal conditions. Nanomaterials 11, 5 (2021): 1351.

[4] Mélinon, P., et al. Playing with carbon and silicon at the nanoscale. Nature materials 6,7 (2007): 479-490.
[5] Yoshida, Minoru, et al. Pressure-induced phase transition in SiC. Physical Review B 48,14 (1993): 10587.
[6] Tian, Dongyu, et al. In situ investigation of nanometric cutting of 3C-SiC using scanning electron microscope. The International Journal of Advanced Manufacturing Technology 115,7 (2021): 2299-2312.
[7] S. Zhao, R. Flanagan, E.N. Hahn, et al., Shock-induced amorphization in silicon carbide, Acta Mater. 158 (2018) 206-213.
[8] Ahmad, et al. Nanoscale elastic-plastic deformation and mechanical properties of 3C-SiC thin film using nanoindentation. International Journal of Applied Ceramic Technology 16.2(2019):706-717.
[9] Alam, Masud, et al. Finite Element Modeling of Brittle and Ductile Modes in Cutting of 3C-SiC. Crystals 11.11 (2021): 1286.
[10] Zhao, Liang, et al. Atomistic origin of brittle-to-ductile transition behavior of polycrystalline 3C–SiC in diamond cutting. Ceramics International 47.17 (2021): 23895-23904.
[11] Mishra, Maneesh, and Izabela Szlufarska. Possibility of high-pressure transformation during nanoindentation of SiC. Acta Materialia 57,20 (2009): 6156-6165.
[12] Goel, Saurav, et al. Anisotropy of single-crystal 3C-SiC during nanometric cutting. Modelling and Simulation in Materials Science and Engineering 21,6 (2013): 065004.
[13] Liao, Dahai, et al. Analysis of Elastic-Plastic Deformation Law on 3C-SiC Ceramic Parts with Different Indenters by Nanoindentation via Molecular Dynamics Simulation. JOM (2022): 1-10.
[14] Reddy, Junuthula Narasimha. Introduction to the finite element method. McGraw-Hill Education, 2019.
[15] Ma, S., X. Zhang, and X. M. Qiu. Comparison study of MPM and SPH in modeling hypervelocity impact problems. International journal of impact engineering 36,2 (2009): 272-282.
[16] Shim, S. , J. I. Jang , and G. M. Pharr . Extraction of flow properties of single-crystal silicon carbide by nanoindentation and finite-element simulation. Acta Materialia 56.15(2008):3824-3832.
[17] Zhang, J. , et al. Brittle-to-ductile transition in elliptical vibration-assisted diamond cutting of reaction-bonded silicon carbide. Journal of Manufacturing Processes 45, Sep.(2019):670-681.
[18] Zhao, Liang, et al. Depth-sensing ductile and brittle deformation in 3C-SiC under Berkovich nanoindentation. Materials & Design 197, (2021): 109223.
[19] Liu, Yao, et al. Smoothed particle hydrodynamics simulation and experimental analysis of SiC ceramic grinding mechanism. Ceramics International 44, 11 (2018): 12194-12203.
[20] Duan, Nian, et al. Analysis of grit interference mechanisms for the double scratching of monocrystalline silicon carbide by coupling the FEM and SPH. International Journal of Machine Tools and Manufacture 120 (2017): 49-60.
[21] Anicode, Vinod, Cagan Diyaroglu, and Erdogan Madenci. Peridynamic Modeling of Damage due to Multiple Sand Particle Impacts in the Presence of Contact and Friction. AIAA Scitech 2020 Forum. 2020.
[22] Silling, Stewart A. Reformulation of elasticity theory for discontinuities and long-range forces. Journal of the Mechanics and Physics of Solids 48,1 (2000): 175-209.

[23] Liu, Ning, Dahsin Liu, and Wu Zhou. Peridynamic modelling of impact damage in three-point bending beam with offset notch. Applied Mathematics and Mechanics 38, 1 (2017): 99-110.
[24] Niazi, Sina, Ziguang Chen, and Florin Bobaru. Crack nucleation in brittle and quasi-brittle materials: A peridynamic analysis. Theoretical and Applied Fracture Mechanics 112, (2021): 102855.
[25] Karpenko, Olena, Selda Oterkus, and Erkan Oterkus. Peridynamic analysis to investigate the influence of microstructure and porosity on fatigue crack propagation in Additively Manufactured Ti6Al4V. Engineering Fracture Mechanics (2022): 108212.
[26] Wu, You, et al. A Peridynamic Model for Dynamic Fracture of Layered Engineered Cementitious Composites. Acta Mechanica Solida Sinica (2022): 1-11.
[27] Shang, S. , et al. A bond-based peridynamic modeling of machining of unidirectional carbon fiber reinforced polymer material. International Journal of Advanced Manufacturing Technology 102, 9 (2019): 4199-4211.
[28] Postek, E., T. Sadowski, and M. Boniecki. Impact of brittle composites: Peridynamics modelling. Materials Today: Proceedings 45, (2021): 4268-4274. [29] Isiet, M. , I. Mikovi , and S. Mikovi . Review of peridynamic modelling of material failure and damage due to impact. International Journal of Impact Engineering 147, (2021): 103740..
[30] Wang, Lanwen, Xuanyu Sheng, and Jianbin Luo. A peridynamic frictional contact model for contact fatigue crack initiation and propagation. Engineering Fracture Mechanics 264, (2022): 108338.
[31] Li, Zhiyuan, et al. Nonlocal steady-state thermoelastic analysis of functionally graded materials by using peridynamic differential operator. Applied Mathematical Modelling 93, (2021): 294-313.
[32] He, Dewei, Dan Huang, and Dongju Jiang. Modeling and studies of fracture in functionally graded materials under thermal shock loading using peridynamics. Theoretical and Applied Fracture Mechanics 111, (2021): 102852.
[33] Cao, Yuzhe, et al. Modeling the nanoindentation response of silicate glasses by peridynamic simulations. Journal of the American Ceramic Society 104, 7 (2021): 3531-3544.
[34] Ebrahimi, Sayna, David Steigmann, and Kyriakos Komvopoulos. Peridynamics analysis of the nanoscale friction and wear properties of amorphous carbon thin films. Journal of Mechanics of Materials and Structures 10, 5 (2015): 559-572.
[35] Silling, S. A. , et al. Peridynamic States and Constitutive Modeling. Journal of Elasticity 88, 2(2007):151-184.
[36] Silling, Stewart A., and Ebrahim Askari. A meshfree method based on the peridynamic model of solid mechanics. Computers & Structures 83, 17-18 (2005): 1526-1535.
[37] Kamensky, David, et al. Peridynamic modeling of frictional contact. Journal of Peridynamics and Nonlocal Modeling 1, 2 (2019): 107-121.
[38] Martins, J. A. C., and J. T. Oden. A numerical analysis of a class of problems in elastodynamics with friction. Computer Methods in Applied Mechanics and Engineering 40, 3 (1983): 327-360.
[39] Huang, Dan, Guangda Lu, and Pizhong Qiao. An improved peridynamic approach for quasi-static elastic deformation and brittle fracture analysis. International Journal of Mechanical Sciences 94, (2015): 111-122.

[40] Parks, Michael L., et al. Peridigm users' guide. Techincal Report SAND2012-7800, Sandia National Laboratories (2012).
[41] Nagappa, Sharvani, Marc Zupan, and C. A. Zorman. Mechanical characterization of chemical-vapor-deposited polycrystalline 3C silicon carbide thin films. Scripta Materialia 59, 9 (2008): 995-998.
[42] Klein, Claude A., and Gregory F. Cardinale. Young's modulus and Poisson's ratio of CVD diamond. Diamond and Related Materials 2, 5-7 (1993): 918-923.
[43] Bobaru, Florin, and Wenke Hu. The meaning, selection, and use of the peridynamic horizon and its relation to crack branching in brittle materials. International journal of fracture 176, 2 (2012): 215-222.
[44] Zhang, Feihu, et al. Friction behavior in nanoscratching of reaction bonded silicon carbide ceramic with Berkovich and sphere indenters. Tribology International 97, (2016): 21-30.
[45] Datye, Amit, and Hua-Tay Lin. Energy analysis of spherical and Berkovich indentation contact damage in commercial polycrystalline silicon carbide. Ceramics International 43, 1 (2017): 800-809.
[46] Qiu, Zhongjun, et al. Crack propagation and the material removal mechanism of glass–ceramics by the scratch test. Journal of the mechanical behavior of biomedical materials 64, (2016): 75-85.

Supplementary Files

This is a list of supplementary files associated with this preprint. Click to download.

- SupplementaryMaterial.doc